Energy, Mines and Resources Canada
Énergie, Mines et Ressources Canada

CANMET

Canada Centre for Mineral and Energy Technology
Centre canadien de la technologie des minéraux et de l'énergie

Mining Research Laboratories
Laboratoires de recherche minière

SOME OBSERVATIONS ON THE ELECTRICAL CHARACTERISTICS OF RADIOACTIVE (^{222}Rn PROGENY) AND NON-RADIOACTIVE AEROSOLS

J. BIGU ELLIOT LAKE LABORATORY Jan. 1990

DIVISION REPORT MRL 89-89(J) Revision of MRL 88-110(J)

Canada

1-12132

SOME OBSERVATIONS ON THE ELECTRICAL CHARACTERISTICS OF RADIOACTIVE (^{222}Rn PROGENY) AND NON-RADIOACTIVE AEROSOLS

J. BIGU ELLIOT LAKE LABORATORY Jan. 1990

DIVISION REPORT MRL 89-89(J) Revision of MRL 88-110(J)

Published in Health Physics, Vol. 58; No. 1 pps 21-36; Jan. 1990.

45 pp

SOME OBSERVATIONS ON THE ELECTRICAL CHARACTERISTICS OF RADIOACTIVE (^{222}Rn PROGENY) AND NON-RADIOACTIVE AEROSOLS

J. Bigu

Elliot Lake Laboratory, CANMET, Energy, Mines and Resources Canada
P.O. Box 100, Elliot Lake, Ontario, Canada

ABSTRACT

The electrical characteristics of ^{222}Rn, ^{222}Rn progeny atmospheres have been investigated. Experiments were conducted in a ^{222}Rn/^{220}Rn Test Facility (RTTF) of the walk-in type using an electrical elutriator of the split-flow variety, originally designed by Johnston. Experiments were carried out with the 'undisturbed' atmosphere, and when this atmosphere was exposed to a source of electrically charged particles produced by a negative ion-generator. Under normal conditions, the average electrical charge of the ^{222}Rn, ^{222}Rn progeny atmosphere was substantially less than one elementary unit. Under the influence of the ion-generator, however, the electrical charge exceeded two elementary units, and the electrical charge distribution was non-symmetrical. It was found that the particle concentration in the RTTF substantially decreased with the operation of the ion-generator.

INTRODUCTION

The short-lived decay products of ^{222}Rn and ^{220}Rn are formed initially in an atomic, positively charged state which rapidly combines with sub-micron aerosols. As aerosols are found in positively, negatively and neutrally charged states, the resulting atmosphere consists of a complex mixture of charged and neutral particles of a size covering a wide range.

Similarly, measurements have shown that industrial dusts in the respirable size range also carry an electrical charge (Patterson et al. 1929: Kunkel 1950a and b; Johnston et al. 1985, 1987). The electrical charge associated with Long-Lived Radioactive Dust (LLRD), i.e., dust containing long-lived radioisotopes, is important in the context of this paper. Long-Lived Radioactive Dust is found in mine air in the course of U mining operations.

The charge associated with radioactive submicron aerosols and LLRD in the respirable size range is of interest from the health physics standpoint since it influences the deposition of these particles in the human respiratory system (Prodi and Mularoni 1985).

Because of the electrical charge associated with the ^{222}Rn and ^{220}Rn progenies, and with LLRD, these radioactive particles can be influenced by external electric and magnetic fields (Fuchs 1964; Jonassen 1983; Bigu 1985 and 1986), thereby providing a means to reduce radiation levels in working areas.

The electrical characteristics of radioactive aerosols in their natural environments and non-radioactive aerosols have been investigated by several workers (Billard and Madelaine 1967; Bricard et al. 1964; Dua et al. 1978; Porstendörfer and Mercer 1979; Dua and Kotrappa 1981; Bigu 1985 and 1986; Hoppel 1985). Work on the electrical behaviour and other characteristics of

^{222}Rn and ^{220}Rn progeny conducted at our laboratory and in underground U mines has been reported elsewhere (Bigu 1983, 1984a, 1985, 1986 and 1988).

This work was aimed at determining the electrical characteristics of an 'undisturbed' ^{222}Rn, ^{222}Rn progeny atmosphere and also to investigate the effect of unipolar charging of this atmosphere by a negative ion-generator. The study was carried out in a $^{222}Rn/^{220}Rn$ Test Facility (RTTF) of the walk-in type. An electrical elutriator of the two split-flow type designed by Johnston el al. (1983) in conjunction with a variety of radioactivity and aerosol measuring instrumentation, was used in this study.

DESCRIPTION OF THE APPARATUS

Except for the RTTF, and the electrical elutriator, the rest of the instrumentation used in this study is commercially available. An early prototype of the RTTF has been described elsewhere (Bigu 1984b). However, the installation presently used in these experiments is a significantly improved, larger, and more flexible version than the one used previously.

The electrical elutriator, hereafter commonly referred to as the Split-Flow Elutriator (SFE), was designed by Johnston (1983) and duplicated at the Elliot Lake Laboratory (Grenier and Butler 1988). A brief description of the elutriator is given below.

The SFE basically consists of two halves that make up the main body of the elutriator, a flow-splitting end cap and two stainless steel parallel plates to which a variable voltage can be applied. The main body and the flow-splitting assembly are made from high-resistivity laminated epoxy resin sheets.

The elutriator channel, lined with the steel plates, is 35 cm in length, 8.6 cm in width, and 0.8 cm in height. Figure 1 shows a side view and a top cut-away view of the SFE (Johnston 1983).

The size of the SFE channel was designed to operate at a nominal flowrate of 3 L min^{-1}. This flowrate permits laminar flow conditions in the channel and provides an air clearance time of less than 5 s.

The particular design of the flow-splitting assembly allows the SFE to be used under two different modes of operation of practical interest, namely, configurations X and Y (see Fig. 2), described below.

EXPERIMENTAL PROCEDURE

The split-flow elutriator (SFE) was used in ^{222}Rn, ^{222}Rn progeny atmospheres produced in the RTTF by means of dry ^{226}Ra sources.* In order to minimize plate-out of the ^{222}Rn progeny on the RTTF walls as well as to provide a substrate for attachment of the ^{222}Rn progeny, aerosols were injected into the RTTF by means of a constant output aerosol atomizer**, in conjunction with an air supply system+, and other associated equipment. Rn-222 from the ^{226}Ra sources was mixed with a NaCl aerosol cloud in a mixing chamber before being injected into the RTTF.

It should be stressed that the SFE cannot distinguish between 'conventional' electrically charged aerosols and electrically charged ^{222}Rn progeny. For this reason it is important to devise a means to ascertain that the electrical charge and electrical charge distribution measured by the SFE correspond to (or are representative of) that of the ^{222}Rn progeny investigated. This can be done using configurations X and Y as illustrated in Fig. 2.

In configuration X (top Fig. 2), all SFE sampling ports were connected together and then split into two flows; one flow was directed to a

---

*Model RN-1025, Pylon Electronic Development, 147 Colonnade Road, Ottawa, Ontario K2E 7L9.
**Model 3076, +Model 3074, Thermo-Systems Inc., (T.S.I.), P.O. Box 43394, St. Paul, MN 55164.

condensation nuclei counter (CNC)*, whereas the other flow (2.7 L min^{-1}) went through an absolute filter, housed in a sample holder, by means of a servo-controlled flow adjustable sampling pump. This experimental arrangement permitted monitoring of aerosol concentrations as well as measurement of ^{222}Rn progeny deposited in the filter by gross α-counting and α-particle spectrometry. Configuration X enabled the study of the electrical characteristics of the 'undisturbed' ^{222}Rn progeny. In this configuration, no electrical polarity discrimination is possible because all SFE sampling ports are connected together.

In configuration Y, the two sampling sites of the SFE were run independently at 3 L min^{-1} each. One side of the SFE flow system was split, as before, into two arms, except that one arm could go either to a CNC or to a Differential Mobility Particle Sizer (DMPS)** in conjunction with a CNC. The DMPS/CNC arrangement was used for aerosol size distribution analysis. The other arm was connected to a sample holder/filter arrangement for radioactivity measurement purposes. The second sampling side of the SFE could be connected to a similar arrangement to that described for the first side, or alternatively to a CNC for aerosol monitoring purposes, or to operate in the conventional way described in the literature (Johnston 1983; Johnston et al. 1985, 1987). It should be noted that configuration Y can also be realized by using one sampling side of the SFE in the manner described above while maintaining the other side at the same airflow by means of an external pump. Charge distribution information can be obtained by alternatively reversing the polarity of the voltage applied to the plates of the SFE or by running a series of measurements with one polarity first, and then reversing the

---

*Model 3020 (0.3 Lmin^{-1}), **Model 3071, Thermo-Systems Inc., (T.S.I.), P.O. Box 43394, St. Paul, MN 55164.

polarity. Configuration Y permits aerosol electrical polarity discrimination.

Configuration Y was used to investigate the electrical characteristics of ^{222}Rn progeny exposed to a source of negatively charged ions produced by a small ion-generator*. The negative ion-generator provided a means to deposit electrical charge on ^{222}Rn progeny. Configuration Y is shown in Fig. 2 (bottom). The aim of this experiment was to determine whether significant electrical charging of the ^{222}Rn progeny would take place under the influence of the negative ion-generator. The latter was a rather simple apparatus that had voltage or current control. The use of a positive ion-generator was also considered but unfortunately it was not available at the time.

Measurements with the SFE were made by varying the external DC voltage applied to the SFE plates between 0 and $\pm$5000 V. The DC voltage was provided by an external DC power supply.

In addition to the above, frequent measurements of aerosol concentration and size distribution in the RTTF were made.

THEORETICAL BACKGROUND

It can be shown that the number of elementary charges, n, on a particle is given by (Johnston 1983, Hochrainer 1985).

$$n = 3\pi\mu\eta D_p/eC \qquad (1)$$

where, η is the air viscosity (~1.8×10^{-5} Kg s^{-1} m^{-1})

D_p is the particle diameter (m)

μ is the particle mobility (m^2 V^{-1} s^{-1})

e is the electron charge (1.602×10^{-19} Coulomb)

C is the Cunningham slip correction (~1)

---

*Model Bionair 100A, Bionair Corporation, 565A Commerce St., Flankling Lakes, NJ 07417.

The mobility of the particle can be obtained from the flowrate conditions and the physical dimensions of the SFE as follows (Johnston 1983):

$$\mu = F(Q/V_o) \tag{2}$$

where, Q is the sampling flowrate ($m^3\ s^{-1}$)

F is a geometrical factor given by b/wl

where, b, w and l are the physical dimensions of the SFE (i.e., w and l, are, respectively, the channel width and the channel length, whereas b is half the SFE channel height. All dimensions in m).

V_o is a voltage defined as follows: particle concentration data are tabulated as a function of voltage differential applied to the SFE. The data are then normalized to zero volt concentration and plotted. A tangent passing through the 50% normalized concentration point defines the voltage V_o by drawing a vertical line to the x-axis from the tangent contact point (see Fig. 3).

Substituting Equation 2 into Equation 1, one gets the number of elementary charges on a particle size D_p:

$$n = 3\pi FK(D_p/V_o) \tag{3}$$

where,

$$K = \eta Q/eC \tag{4}$$

Taking into account that for the SFE used here, $w = 8.6 \times 10^{-2}$ m, l = 0.35 m, and $b = 4 \times 10^{-3}$ m, it can be shown that Equation 3 reduces to:

$$n = 7.036 \times 10^{9}\ (D_p/V_o) \tag{5}$$

where, D_p is in m.

The procedure outlined above (Johnston 1983) can be applied to particles of different sizes in an aerosol or dust cloud in order to obtain the electrical charge distribution of the cloud. This procedure is straightforward for clouds with symmetrical charge distributions. However, for non-symmetrical charge distributions, the procedure is more complex, as described elsewhere (Johnston 1983).

RESULTS AND DISCUSSION

It is important in the context of the data presented here to distinguish between the meaning given in this paper to 'total' aerosol and radioactive aerosol. In the first category both radioactive (in this case ^{222}Rn and its progeny) and non-radioactive aerosols are included, whereas in the second category only ^{222}Rn progeny aerosols (free or attached to other non-radioactive aerosols) are considered. Although it should be evident that radioactive and non-radioactive aerosols are all part of the same particle distribution, the above terminology is useful and justifiable because the radioactive aerosol distribution can, in fact, be determined experimentally (see below), and hence, distinguished from non-radioactive aerosols.

Because the SFE cannot distinguish between the two categories on the basis of charge, an experimental protocol was designed, as previously indicated, to identify, characterize, and quantify both components, namely the radioactive and non-radioactive aerosol fractions in the 'total' aerosol cloud. For simplicity, the experimental data will be divided into the following groups:

a) Electrical characteristics of the total aerosol cloud, without external electrical influence, i.e., no ion-generator;
b) Electrical characteristics of the radioactive aerosol cloud, without external electrical influence, i.e., no ion-generator;
c) Electrical characteristics of the total aerosol cloud under the influence of an ion-generator; and
d) Electrical characteristics of the radioactive aerosol cloud under the influence of an ion-generator.

A. ELECTRICAL CHARACTERISTICS OF TOTAL AEROSOL (NO ION-GENERATOR)

Figures 3 to 5, and Tables 1 and 2 show data obtained using the SFE in configuration X in conjunction with the CNC (Fig. 2), and the DMPS/CNC arrangement (Fig. 4 and 5).

Figure 3 shows the total aerosol concentration versus high voltage (H.V.). Only the negative portion of the graph is shown because the aerosol cloud was symmetrical with respect to charge. (The same was found to hold true for the radioactive aerosol, where Table 2 shows the ^{222}Rn progeny concentration versus several positive and negative values of the H.V. on the SFE to illustrate this point.)

Figure 4 shows the total aerosol concentration size distribution for two SFE voltage conditions, namely 0 V and -2000 V. This Figure and Table 1 show that the geometric mean (G.M.) of the size distribution after passing through the SFE decreases with increasing voltage. For the particular experimental conditions, an example is given in Fig. 4, a decrease in G.M. of ~19% was brought about by the application of -2000 V. The percentage reduction in the G.M. of the aerosol cloud depends on the voltage applied to the SFE, experimental conditions, type of aerosol, water vapour content, and possibly other characteristics of the aerosol cloud, in a little understood fashion.

A decrease in the G.M. of the aerosol cloud suggests the removal of the larger particle size fraction from the aerosol size distribution. However, as the electrical force exerted on a charged particle is proportional to the electrical charge on the particle, a reduction in G.M. of the charged aerosol cloud can be interpreted as the removal of the fraction of particles with higher electrical charge. Hence, from particle size and electrical charge (on the particle) considerations one may surmise that Fig. 4 and Table 1

demonstrate that under our experimental conditions large particles carry, in general, more charge than smaller particles.

A value for the electrical charge of the aerosol cloud can be estimated from Fig. 3 by following Johnston's graphical procedure described elsewhere (Johnston 1983; Johnston et al. 1985). This procedure consists of drawing a straight line from the y-axis corresponding to $N_0/2$ (where N_0 is the total aerosol concentration corresponding to 0 V) tangent to the aerosol concentration (N) versus H.V. curve. The intersection point is then projected onto the x-axis where the corresponding voltage, V_0, is read. The voltage so obtained is then substituted into Equation 5 in order to obtain n, the electrical charge. Figure 3 gives $V_0 \sim 4 \times 10^3$ V. Because the electrical response of the SFE was symmetrical relative to polarity (see Table 2), V_0 will be positive or negative according to the polarity applied to the SFE plates (see Fig. 3). Hence, n will be the same irrespective of sign (see Equation 5).

Because Fig. 3 has been obtained with a CNC (which measures aerosol concentration but provides no particle size distribution information, except for approximate lower and upper particle size operating limits), the value for n is not defined unless a definite particle size is chosen to describe the aerosol cloud. An obvious choice is the G.M. of the aerosol cloud. Taking G.M. = 0.09 μm, as an approximate value based on experimentation, and H.V. = 5×10^3 V, and substituting this value into Equation 5, one gets:

$$n = 7.036 \times 10^9 \ (0.09 \times 10^{-6}/4 \times 10^3) \sim 0.16$$

Since the electrical charge on a particle is either 0 or an integer, values for n less than unity suggest that a fraction of the aerosol cloud carries no electrical charge. Figure 3 indicates that over 50% of the aerosol cloud is electrically charged (most likely >60% if the line is extrapolated to H.V. $> 5 \times 10^3$ V). This value is consistent with other experimental work by

the author (Bigu 1985; Bigu and Grenier 1986).

As indicated above, the value n ~0.16 obtained above is not truly representative of the electrical charge of the aerosol cloud because particle size distribution information is not given. A more accurate electrical charge description of the aerosol cloud can be obtained by substituting the CNC by the DMPS/CNC arrangement, and conducting a similar kind of analysis covering the entire particle size range in small particle size increments. The result of such analyses is summarized in Fig. 5 where n (see Equation 5) is plotted versus D_p (particle size, μm). This graph shows that the electrical charge on the particle varies with particle size ranging from ~0.15 for D_p ~0.07 μm to ~1.2 for D_p ~0.34 μm. Data for $D_p > 0.35$ μm are not reliable because of the low particle concentration in this size range, and hence, poor statistics of counting. The decrease of n for $D_p > 0.3$ μm is not clearly understood, but may be caused by a combination of poor counting statistics, bias of the DMPS, and other as yet unknown factors. Figure 5 shows that except for $D_p > 0.35$ μm, the particle electrical charge increases with the particle size.

B. ELECTRICAL CHARACTERISTICS OF RADIOACTIVE AEROSOLS (NO ION-GENERATOR)

Figures 6 and 7, and Tables 1 and 2 show radioactive aerosol data using the SFE in configuration X (Fig. 2, top). The sampling filter was used to collect radioactive aerosol, i.e., ^{222}Rn progeny, and the DMPS/CNC to gather, concurrently, total aerosol and particle size distribution data (Table 1). Radioactive aerosol was sampled for 5 min at a time at different H.V. and the α-particle activity was measured by α-spectrometry using a silicon-barrier detector, and associated electronic circuitry, in conjunction with a multichannel analyzer. The spectra so obtained (i.e., ^{218}Po and ^{214}Po photopeaks) were used in the analysis. Rn-222 progeny and total aerosol data are shown in Table 1 and plotted in Fig. 6. It should be noted that the

integrated α-particle count under the ^{218}Po and ^{214}Po photopeaks as well as the total α-count, i.e., ^{218}Po + ^{214}Po, have been plotted independently in Fig. 6. The normalized α-counts are, however, very similar and for all practical purposes they can be considered identical. Because of this, a single line passing through all ^{222}Rn progeny data points has been drawn.

An estimate for the electrical charge of the ^{222}Rn progeny aerosol cloud can be obtained by applying Johnston's method to the α-particle count following the same procedure as for the total aerosol concentration (see case A and Fig. 3). The value obtained for V_o is ~1640 V (see Fig. 6). Unfortunately, the experimental arrangement used did not allow for the ^{222}Rn progeny size distribution to be determined. This can be done using diffusion batteries of the screen, parallel plate, or concentric type. However, concurrent ^{222}Rn progeny size distribution measurements would have made the present experiment far too complex as not all the necessary variables of interest could have been determined simultaneously.

It is well known that for a lognormal aerosol distribution ^{222}Rn progeny attach themselves preferentially to airborne particles in the submicron size range (<0.1 to ≲0.2 μm) (Mercer and Stowe 1971). This value and the G.M. for the total aerosol cloud are similar enough so that D_p ~0.1 μm can be taken in the calculations for comparison purposes. Using Equation 5, one obtains n ~0.43 for ^{222}Rn progeny. For the total aerosol cloud, V_o~ 4 x 10^3 V (see Fig. 3 and 6), hence n ~0.16 is obtained. Assuming similar size distributions for the total aerosol and ^{222}Rn progeny clouds, the above results suggest that ^{222}Rn progeny carry an electrical charge ~2.5 times larger than 'normal' (i.e., non-radioactive) aerosol. This result can be understood because of aerosol self-charging effects caused by radioactive decay (Yeh 1976). Furthermore, because the electrical charge carried by ^{222}Rn progeny must be either 0 or an integer, n < 1 indicates that a fraction of the

^{222}Rn progeny cloud carries no electrical charge. From Fig. 6 it can be seen that about 65% of the ^{222}Rn progeny is either positively or negatively charged whereas the remaining fraction (~35%) is in a neutrally charged state. These data are consistent with other measurements by the author (Bigu 1985, 1986).

Figure 7 shows ^{222}Rn progeny spectra at three different voltages, namely, 0 V, -500 V, and -2000 V. The spectra show a decrease of the ^{218}Po and ^{214}Po photopeaks with increasing H.V., as previously discussed (Table 1 and Fig. 6). No significant spectral difference as measured by the ratio $^{218}Po/^{214}Po$ were found.

Table 2 shows that N and ^{222}Rn progeny data are equally affected by a given H.V. either positive or negative. Other relevant data are also shown in this Table.

From Figures 6 and 7, and Tables 1 and 2, one may tentatively surmise:

1. The electrical charge on ^{222}Rn progeny appears to be significantly larger than that corresponding to the total aerosol cloud;
2. Both ^{218}Po and ^{214}Po are electrically charged;
3. About 65% of the ^{222}Rn progeny are electrically charged either positively or negatively.

C. ELECTRICAL CHARACTERISTICS OF TOTAL AEROSOL UNDER THE INFLUENCE OF AN ION-GENERATOR

In this study, the total aerosol cloud was exposed to a negative ion-generator (IG) in order to induce charge effects, i.e., to deposit electrical charge on the particles forming the cloud. Particle size and charge distributions of the aerosol cloud under the influence of the ion-generator were determined. The effect of the ion-generator could not be anticipated because of the lack of technical information by the manufacturer of the IG. The manufacturer claims that the IG produces a large excess of negative ions.

However, the kind of ions, particle size and electrical charge distributions are not available.

In this study it was important to determine the electrical polarity of the particles. Hence, configuration Y (Fig. 2, bottom) was used. The results of this investigation are shown in Fig. 8 to 10, and Tables 3 and 4.

Figure 8 shows the aerosol concentration, N, measured with the CNC versus positive and negative voltage applied to the SFE. Contrary to data obtained without the IG, the experimental results obtained using the IG are markedly charge asymmetric.

Although the DMPS/CNC apparatus was used occasionally in this series of experiments, the data shown in Fig. 8 were obtained with the CNC. The relatively long time required by the DMPS/CNC apparatus to acquire, process, and print-out particle mobility and size distribution data was not particularly suitable for the experiment with the IG where a large number of measurements had to be carried out in a short time with the IG on and off, and within a wide range of positive and negative values for the voltage. Hence, the analysis that follows from Fig. 8 is done by taking the G.M. of the aerosol cloud (i.e., ~0.085 μm as determined by the DMPS/CNC arrangement). This value for the G.M. represents an average because it varies with experimental conditions, e.g., operation of the IG. (A more accurate procedure would have entailed a series of similar measurements for each particle size using the DMPS/CNC apparatus. The reasons for not having done so have been given above.)

Because of the asymmetrical nature of the graph describing N versus positive and negative H.V., the simple graphical procedure used before to obtain V_o and, hence, n, can no longer be applied. In the present case 'deconvolution' of the data of Fig. 8 was done using a graphico-analytical method developed by Johnston (1983) designed to deal with charge asymmetric

situations. The result of this analysis is presented in Fig. 9. The following are some definitions to clarify the meaning of the above illustration using Johnston's procedure. For further information the reader is urged to refer to the original publication.

The symbol A stands for A-type experimental 'run', and indicates data obtained when both channels of the split-flow elutriator (SFE) are directed to the aerosol counter, e.g., CNC (see configuration X of Fig. 2). Data tabulated under A represent values of the tangent intercept points from the type A curve.

The symbols B^+ and B^- refer to data obtained when the aerosol counter samples from the exit channel on the side of the positive and negative electrode of the SFE, respectively (see configuration Y of Fig. 2). Data tabulated under B^+ and B^- curves represent values of the tangent intercept points on the type B^+ and B^- curves, respectively (see Fig. 9). (Note: because of space limitations and simplicity, Tables for A, B^+ and B^- are not included in this paper.)

Figure 9 shows that a large fraction of the aerosol cloud is charged negatively under the influence of the ion-generator with an electrical charge of about 2.34 $\pm$ 0.5 elementary units corresponding to particles with electrical mobility of ~2.5 x 10^{-8} m^2 V^{-1} s^{-1}. (If, for rough comparison purposes, the simplified graphical analysis used in Sections A and B is applied to the positive and negative voltage portions of Fig. 8 independently, the following, respective, values for V_o are obtained using Equation 5 for D_P = 0.085 μm: $V_o(+)$ = 1.5 and $V_o(-)$ = 3.0. The mean value of $V_o(+)$ and $V_o(-)$ is 2.25 which does not differ much from n = 2.34 $\pm$ 0.5 given above. Alternatively, n = 2.34 $\pm$ 0.5 obtained by the rigorous method is somewhere between $V_o(+)$ and $V_o(-)$.)

Figure 10 shows the total aerosol size distribution in the RTTF

(bypassing the SFE) when the IG is off (top left hand side histogram) and when the IG is operating (bottom left hand side histogram). The right hand side histograms of Fig. 10 show the total aerosol size distribution using the SFE when a voltage of -5000 V is applied with the IG off (top histogram), and when the IG is on (bottom histogram).

The data of Fig. 10 show that the aerosol concentration in the RTTF is reduced by the operation of the IG, an experimental fact that has been observed by the author in the course of several studies (Bigu 1983, 1984a and 1988). The reduction in aerosol concentration was in the range 10-20% (see also Table 3) with no apparent significant difference in the G.M. of the distribution. The latter is to be expected because of the limited ion output of the IG and the relatively large volume of the RTTF (~30 m^3). The modest reduction in N in the RTTF is consistent with the above, and hence the constancy of G.M.. The reduction in aerosol concentration in the RTTF when the IG was on is attributed to an increase in charged aerosol plated-out on the RTTF walls. (Plate-out of charged aerosols on plastic tubing walls, and other apparatus surfaces could also contribute significantly but this effect has not been investigated here, and hence is an unknown variable.)

A considerable reduction (10-20 fold) in aerosol concentration was observed at the outlet of the SFE in the voltage range 0 to -5000 V when the IG was operated in close proximity to the SFE (see Table 4). Furthermore, the G.M. of the aerosol distribution exiting the SFE was significantly reduced (~30% for H.V. ~ -5000 V, ~20-25% for H.V. = 0 V) by the operation of the IG (see bottom of Table 4). This effect persisted even at 0 voltage where an average G.M. ~0.0877 μm was obtained when the IG was off compared with a value of 0.0661 μm when the IG was on.

The observed reduction in N and G.M. of the irradiated aerosol cloud when using the SFE can, tentatively, be interpreted as the product of

clustering, condensation or coagulation of small charged and neutral particles into larger (charged) ones, which are, therefore, more easily removed by the SFE on account of their larger electrical charge on their surface. The net effect of the IG in the RTTF is a reduction in N (which has been experimentally verified as indicated above), and an increase in G.M. which can indirectly be inferred from SFE data.

The effect of the IG on N versus voltage (H.V.) is also shown in Fig. 12 (which also shows the total ^{222}Rn progeny α-particle count as discussed in Section D, below). An estimate of the electrical charge on the aerosol cloud calculated for the negative voltage portion of the Figure and Equation 5, assuming G.M. ~0.085 μm, gives n ~ 2.7 elementary unit charges, which is in fair agreement with other values given above.

D. ELECTRICAL CHARACTERISTICS OF RADIOACTIVE AEROSOLS UNDER THE INFLUENCE OF AN ION-GENERATOR

Data regarding the electrical characteristics of ^{222}Rn progeny in the RTTF have been summarized in Fig. 11 to 13 and Table 4. As for total aerosol, the characteristics of the ^{222}Rn progeny under the influence of the IG were investigated using the SFE in configuration Y. However, because of severe practical constraints, experimental difficulties and time limitations, the polarity of the radioactive aerosol could not be investigated in detail as in Section C for the total aerosol. Hence, data obtained when negative voltages were applied to the SFE are presented here. The analysis carried out with these data is similar to that of sections A and B.

Figure 11 shows the normalized α-particle count versus H.V. for ^{218}Po, ^{214}Po, and ^{218}Po + ^{214}Po, i.e., total α-count under the two photopeaks, denoted by $N_{\alpha,T}$. As for the case discussed in Section B, ^{222}Rn progeny were analyzed by α-spectrometry. Figure 12 shows $N_{\alpha,T}$ versus H.V. Also shown in

this graph, for comparison purposes, is the total aerosol concentration versus H.V..

Calculation of the electrical charge for the ^{222}Rn progeny, assuming D_P ~G.M. = 0.085 - 0.1 μm (see Table 4 and other calculations in this paper), and applying the values for V_o obtained from Fig. 11 to Equation 5, gives n ~2.4 to 3.5 for the electrical charge on ^{222}Rn progeny under the influence of the ion-generator. The above range of values for n is significantly higher than that obtained with the IG off (see Section B).

Figure 12 shows the normalized total aerosol concentration (N) and total α-particle activity ($N_{\alpha,T}$) versus voltage (H.V.) for an experiment in the RTTF with the IG on. For this particular experiment $n(N_{\alpha,T}) < n(N)$ ~4.0.

Because of the inherent error associated with the graphical method and other considerations regarding particle size distribution discussed earlier, the results given above are only approximate and may be expected to vary depending on aerosol composition, method of aerosol production, local environmental conditions in the RTTF, water content of the aerosol cloud, and other factors.

Figure 13 shows ^{222}Rn progeny α-particle spectra obtained using the SFE with no voltage for the IG off (top graph) and when the IG has been operating for a short period (bottom graph). A dramatic decrease in ^{222}Rn progeny collected on the sampling filter can be observed, caused by the operation of the IG (see also Table 4). This decrease in α-particle activity is attributed to the electrical charge imparted to the ^{222}Rn progeny by the IG, which greatly facilitates the plate-out of the latter on the SFE electrodes.

CONCLUSIONS

Some of the main conclusions that can be derived from this study are the following:

1. For the undisturbed aerosol cloud (i.e., IG off), the electrical charge distribution was symmetrical. Furthermore, the electrical charge measured was within the range 0 <n <1 with n(total aerosol cloud) <n(^{222}Rn progeny). Furthermore, ~50% of the total aerosol cloud and ~65% of the radioactive aerosol (^{222}Rn progeny) were electrically charged as evidenced by SFE data;
2. For the disturbed aerosol cloud (i.e., IG on), the electrical charge was non-symmetrical. Over 90% of the cloud was electrically charged with an average charge, n >2. Furthermore, the total aerosol and ^{222}Rn progeny concentrations in the RTTF decreased and the G.M. of the total aerosol cloud increased. The latter is attributed, as previously indicated, to clustering effects caused by the additional charge deposited by the IG on radioactive and non-radioactive aerosols.

It should be noted that an increase in particle (radioactive and non-radioactive aerosol) plate-out on the RTTF walls and the SFE plates, caused by the operation of the ion-generator, has not been considered here, but should not be ignored. Because of practical constraints, no concurrent plate-out measurements were conducted in order to ascertain the importance of this phenomenon on the effects observed. A continuation of the present studies with different kinds of instrumentation is in progress in order to further verify and improve the data presented here. Plate-out measurements are planned to determine its role on the phenomena subject of this paper.

ACKNOWLEDGMENTS

The author would like to thank E. Edwardson for his experimental assistance in this project. Thanks are also extended to M. Grenier, who duplicated Johnston's SFE apparatus in our laboratory, for helpful discussions regarding the performance of the spectrometer.

REFERENCES

Bigu, J. On the effect of a negative ion generator and a mixing fan on the plate-out of radon decay products in a radon box. Health Phys. 44:259-266; 1983.

Bigu, J.; Grenier, M. On the effect of a negative ion generator and a mixing fan on the attachment of thoron-decay products in a thoron box. Health Phys. 46|:933-939; 1984a.

Bigu, J. A walk-in radon/thoron test facility. Am. Ind. Hyg. Assoc. J. 45:525-532; 1984b.

Bigu, J. Effects of electric fields on ^{220}Rn progeny concentration. Health Phys. 49:512-516; 1985.

Bigu, J.; Grenier, M. Electrical characteristics of the short-lived decay products of thoron in underground uranium mines. Am. Ind. Hyg. Assoc. J. 47:308-311; 1986.

Bigu, J. Effect of selected variables on airborne ^{220}Rn progeny concentrations. Health Phys. 54:93-98; 1988.

Billard, F; Madelaine, G. Etude de la charge electrique portee par les aerosols. In: Assessment of airborne radioactivity, proceedings of a symposium held by the International Atomic Energy Agency. Vienna: IAEA; EAEA-SM-95/13; 1967: 325-333.

Bricard, J.; Renoux, A; Pradel, J; Madelaine, G. Spectre des aerosols naturels radioactifs. In: La pollution radioactive des milieux gazeux. pp 15-17; 1964.

Dua, S.K.; Kotrappa,P.; Bhanti, D.P. Electrostatic charge on decay products of thoron. Am. Ind. Hyg. Assoc. J. 39:339-345; 1978.

Dua. S.K.; Kotrappa, P.; Comment on the charge on decay products of thoron and radon. Am. Ind. Hyg. Assoc. J. 42:242-243; 1981.

Fuchs, N.A. The mechanics of aerosols. 2nd ed. New York: The Macmillan Company; 1964.

Grenier, M.G.; Butler, K. Evaluation of a split-flow elutriator used in the determination of airborne dust charge distributions. Elliot Lake Laboratory (CANMET, Energy, Mines and Resources Canada); 1988. Ottawa, Canada. Mining Research Laboratories Division Report MRL 87-187(TR).

Hochrainer, D. Measurement methods for electric charges on aerosols. Ann. Occup. Hyg. 29:241-249; 1985.

Hoppel, W. Ion-aerosol attachment coefficients, ion depletion, and the charge distribution on aerosols. J. of Geophys. Res. 90:5917-5923; 1985.

Johnston, A.M. A semi-automatic method for the assessment of electric charge carried by airborne dust. J. Aerosol Sci. 14:643-655; 1983.

Johnston, A.M.; Vincent, J.H.; Jones, A.D. Measurements of electric charge for workplace aerosols. Ann. Occup. Hyg. 29:271-284; 1985.

Johnston, A.M.; Vincent, J.H.; Jones, A.D. Electrical charge characteristics of dry aerosols produced by a number of laboratory mechanical dispensers. Aerosol Sci. & Tech. 6:115-127; 1987.

Jonassen, N. The effect of electric fields on ^{222}Rn daughter products in indoor air. Health Phys. 45:487-491; 1983.

Kunkel, W.B. The static electrification of dust particles on dispersion into a cloud. J. Appl. Phys. 21:820-832; 1950a.

Kunkel, W.B. Charge distribution in coarse aerosols as a function of time. J. Appl. Phys. 21:833-837; 1950b.

Mercer, T.T.; Stowe, Wm. Radioactive aerosols produced by radon in room air. In: Walton, W.H., editor. Inhaled particles III, volume 2. Surrey (England) Unwin Bros. Ltd. 839-851; 1971.

Patterson, H.S.; Whytlaw-Gray, R.; Cawood, W. The structure and electrification of smoke particles. Proc. Roy. Soc. A 124:523-532, 1929.

Porstendörfer, J.; Mercer, T.T. Influence of electric charge and humidity upon the diffusion coefficient of thoron decay products. Health Phys. 37: 191-199; 1979.

Prodi, V; Mularoni, A. Electrostatic lung deposition experiments with humans and animals. Ann. Occup. Hyg. 29:229-240; 1985.

Yeh, H. A theoretical study of electrical discharging of self-charging aerosols. J. Aerosol Sci. 7:343-349; 1976.

Time	HV (volt)	N (cm^{-3})	$D_P(N_{max})$ (μm)	G.M. (μm)	S	$N_\alpha(^{218}Po)$ (α-count)	$N_\alpha(^{214}Po)$ (α-count)	$N_{\alpha,T}$ (α-count)
17:26	1	9375	0.081	9.81×10^{-2}	1.752	595	2250	3056
12:02	-1	9039	0.124	0.102	1.808	651	2392	3121
16:57	-1500	4820	0.081	8.63×10^{-2}	1.793	265	955	1279
16:32	-750	5305	0.081	9.20×10^{-2}	1.829	298	1286	1680
16:05	-500	5830	0.081-0.124	9.69×10^{-2}	1.829	340	1358	1807
15:37	-300	6436	0.124	0.1	1.805	388	1533	2038
15:10	-1	8213	0.081	0.1	1.763	489	1941	2561
14:43	-5000	4600	0.081	8.56×10^{-2}	1.743	240	783	1096
14:15	-4000	4546	0.081	8.58×10^{-2}	1.758	220	770	1061
13:46	-3000	4446	0.081	8.65×10^{-2}	1.766	223	782	1086
13:17	-2000	4387	0.081	8.77×10^{-2}	1.79	188	788	1044
12:51	-1000	4526	0.081	9.36×10^{-2}	1.856	252	1007	1368
12:19	-500	5221	0.081-0.124	0.102	1.874	332	1325	1736

Notes: IG stands for ion-generator, N stands for aerosol concentration. The symbol $D_P(N_{max})$ is used to indicate the particle size corresponding to the maximum N in the aerosol cloud. THe symbols G.M. and S are used to indicate geometric mean and spread, respectively. HV stands for high voltage. The symbol N_α indicates α-count under the α-particle photopeak(s). The index T denotes total.

Table 1. Aerosol and ^{222}Rn progeny data obtained with the split-flow elutriator (no ion-generator used).

Time	HV (volt)	N (cm^{-3})	$D_P(N_{max})$ (μm)	G.M. (μm)	S	$N_\alpha(^{218}Po)$ (α-count)	$N_\alpha(^{214}Po)$ (α-count)	$N_{\alpha,T}$ (α-count)
11:50	0	9175	0.081	9.40×10^{-2}	1.754	617	2383	3230
12:17	-500	5364	0.081,0.124	9.31×10^{-2}	1.841	404	1443	2000
12:41	+500	5441	0.081,0.124	9.18×10^{-2}	1.841	379	1417	1952
13:05	+1000	4803	0.081	8.36×10^{-2}	1.826	293	1075	1472
13:32	-1000	4832	0.081	8.37×10^{-2}	1.830	265	1055	1471
14:47	-2000	4711	0.081	7.95×10^{-2}	1.775	231	914	1239
15:15	+2000	4700	-	-	-	230	918	1242

Notes: IG stands for ion-generator, N stands for aerosol concentration. The symbol $D_P(N_{max})$ is used to indicate the particle size corresponding to the maximum N in the aerosol cloud. The symbols G.M. and S are used to indicate geometric mean and spread, respectively. HV stands for high voltage. The symbol N_α indicates α-count under the α-particle photopeak(s). The index T denotes total.

Table 2. Effect of the split-flow elutriator electrical polarity on aerosol and ^{222}Rn progeny.

Time	N (cm^{-3})	N_{nor}	IG	$D_P(N_{max})$ (μm)	G.M. (μm)
12:48	8103	0.787	ON	0.107	0.0917
13:56	8135	0.790	ON	0.093	0.0906
14:45	9622	0.934	OFF	0.107-0.124	0.0897
15:33	9175	0.891	ON	0.093-0.107	0.0911
16:36	10300	1.000	OFF	0.093-0.107	0.0890

Notes: N stands for aerosol concentration. N_{nor} represents the normalized aerosol concentration relative to the maximum N measured. The symbol IG stands for ion-generator, $D_P(N_{max})$ represents the diameter corresponding to the maximum aerosol concentration in the aerosol cloud. G.M. stands for geometric mean.

Table 3. Effect of a negative ion-generator on aerosol concentration in a $^{222}Rn/^{220}Rn$ test facility (RTTF) of the walk-in type. No SFE used.

Time	HV (volts)	N (cm^{-3})	$D_p(N_{max})$ (μm)	G.M. (μm)	S	$N_\alpha(^{218}Po)$ (α-count)	$N_\alpha(^{214}Po)$ (α-count)	$N_{\alpha,T}$ (α-count)	Remarks
16:12	0	5070	0.124	0.102	1.725	433	1198	1866	IG ON
17:55	-100	2097	0.124	0.116	1.713	206	842	1108	"
17:28	-200	768	0.124	0.108	1.864	74	298	396	"
17:02	-300	421	0.081	9.31×10^{-2}	1.988	29	129	187	"
16:38	-500	278	0.052	7.07×10^{-2}	2.048	9	73	85	"
15:40	0	8955	0.081	9.21×10^{-2}	1.771	577	2180	2923	IG OFF
11:15+	0	7797	0.093	8.84×10^{-2}	1.74	-	-	2648	"
11:38+	-5000	4005	0.081	7.74×10^{-2}	1.738	-	-	1182	"
12:21+	-5000	411	0.045-0.081	5.53×10^{-2}	1.712	-	-	52	IG ON

Notes: IG stands for ion-generator, N stands for aerosol concentration. The symbol $D_p(N_{max})$ is used to indicate the particle size corresponding to the maximum N in the aerosol cloud. The symbols G.M. and S are used to indicate geometric mean and spread, respectively. HV stands for high voltage. The symbol N_α indicates α-count under the α-particle photopeak(s). The index T denotes total.

+ Data obtained 25 September 1987. Other data collected 30 September 1987.

Table 4. Aerosol and ^{222}Rn progeny data obtained with the split-flow elutriator and with the ion-generator on.

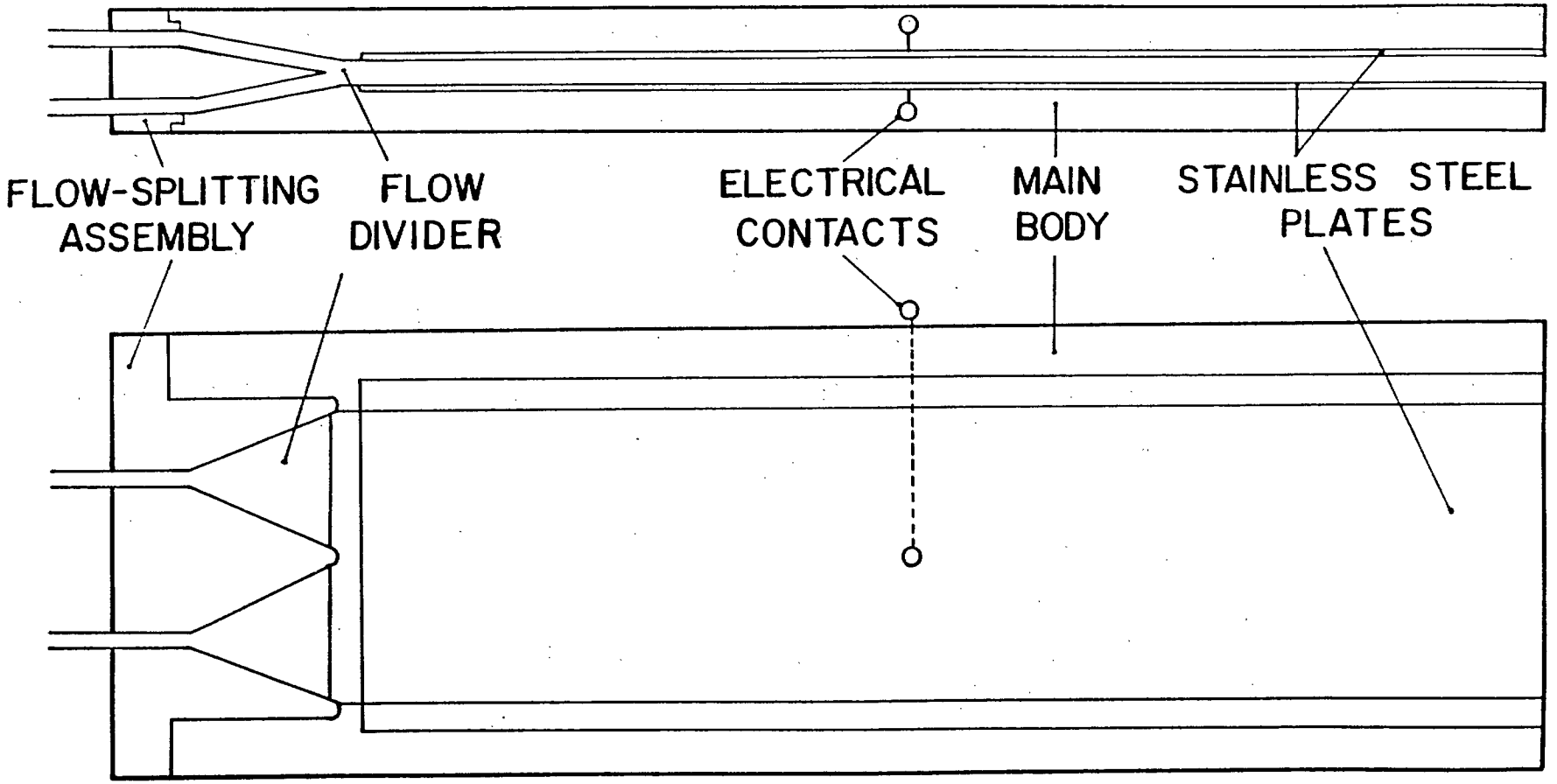

Figure 1. Cut-away views of the split-flow elutriator (SFE).

Figure 1

CONFIGURATION X

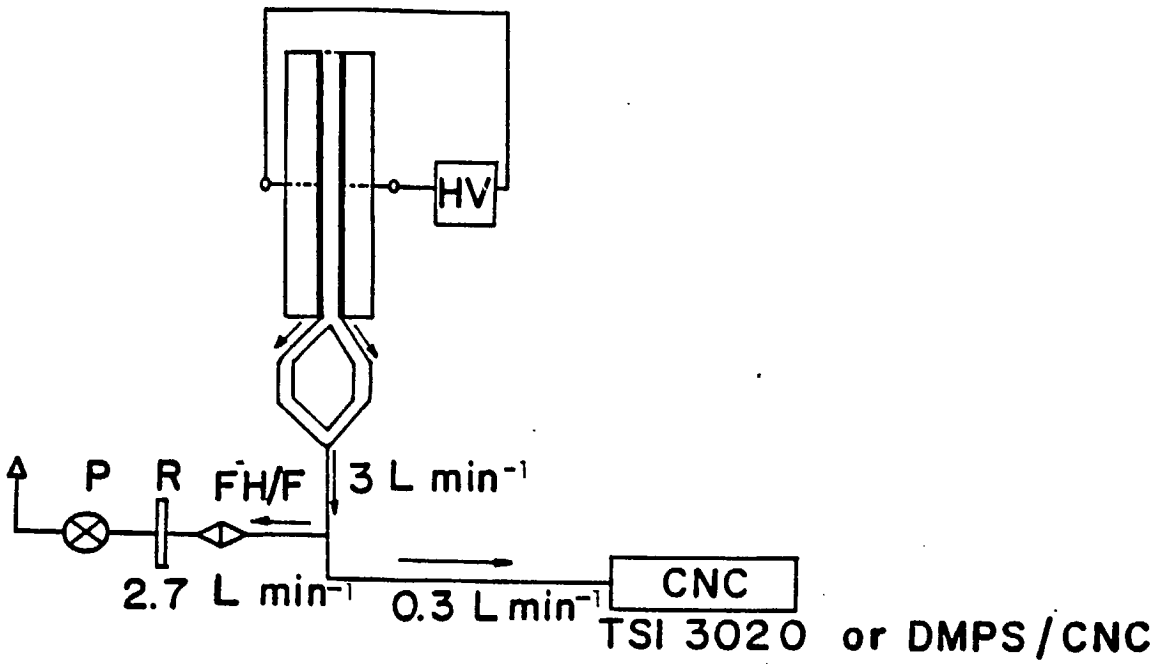

CONFIGURATION Y

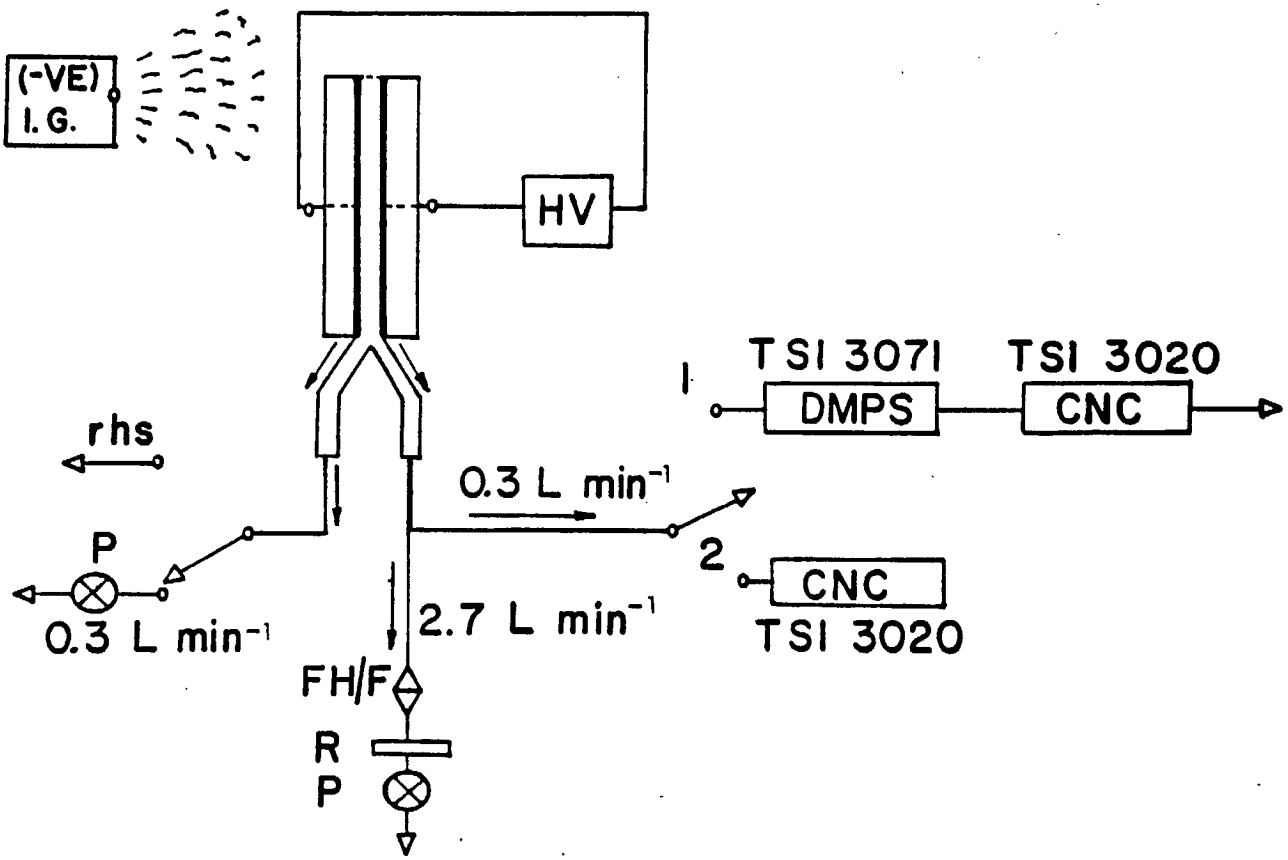

Figure 2. Experimental apparatus. P, R, FH, and F stand, respectively, for pump, rotameter, filter holder and filter.

Figure 3

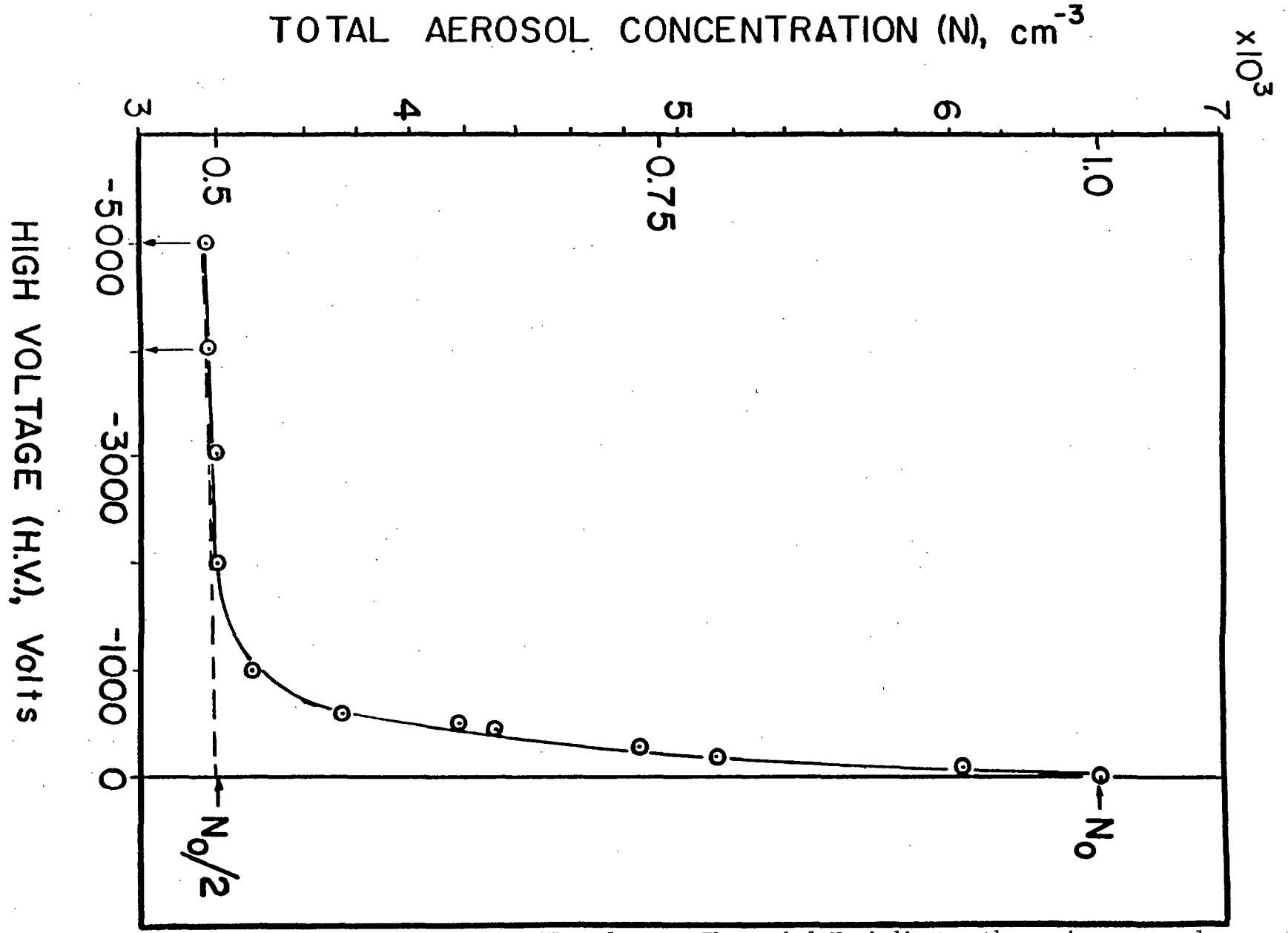

Fig. 3 - Total aerosol concentration versus SFE voltage. The symbol N_o indicates the maximum aerosol concentration. The values on the right hand side scale of the y-axis indicate normalized values for the aerosol concentration. The dotted line is the tangent line to the curve, drawn from the point $N_o/2$, to determine V_o (see text).

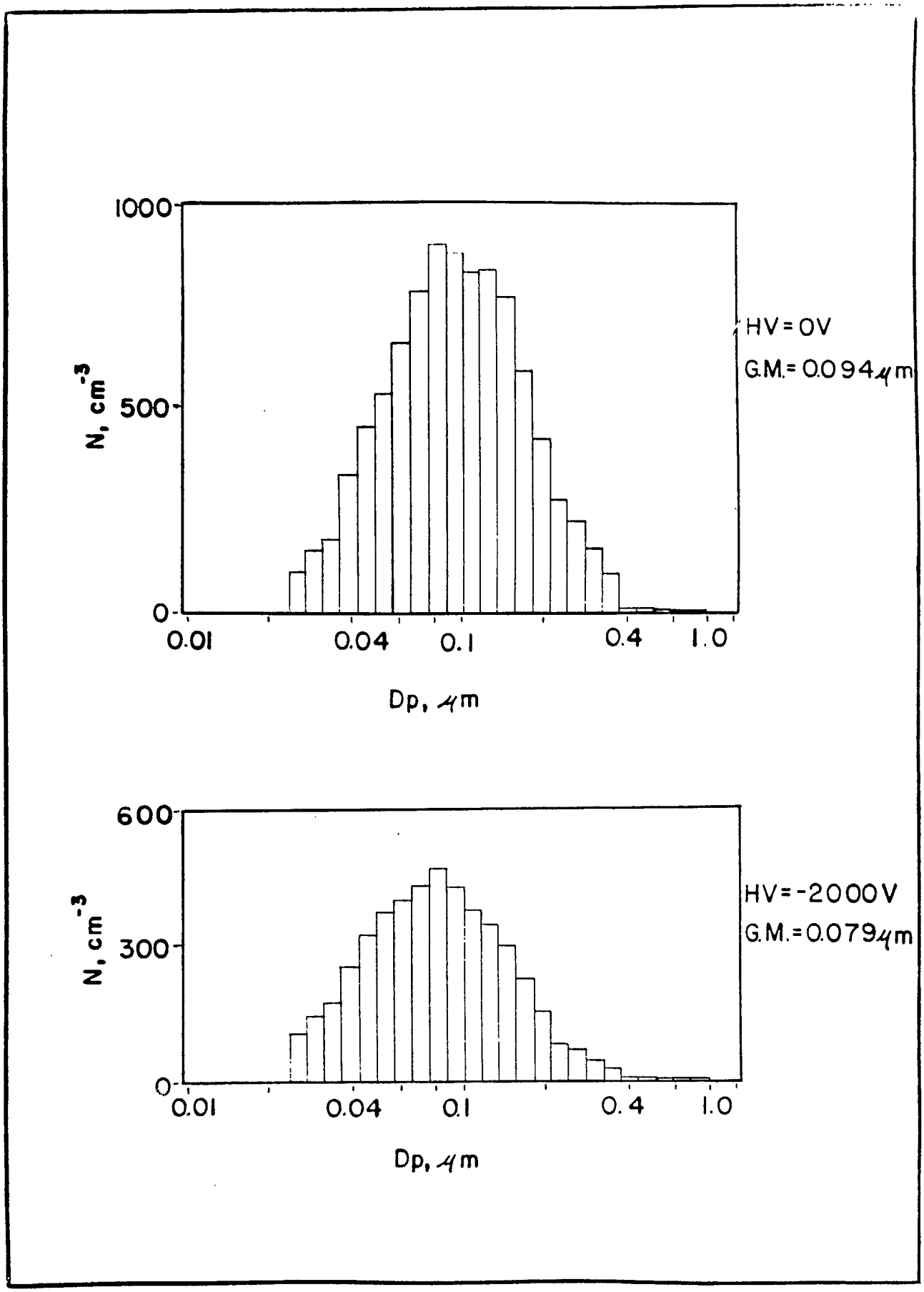

Figure 4. Total aerosol size distribution at the outlet of the SFE for two different SFE voltages. Date obtained with the DMPS/CNC system.

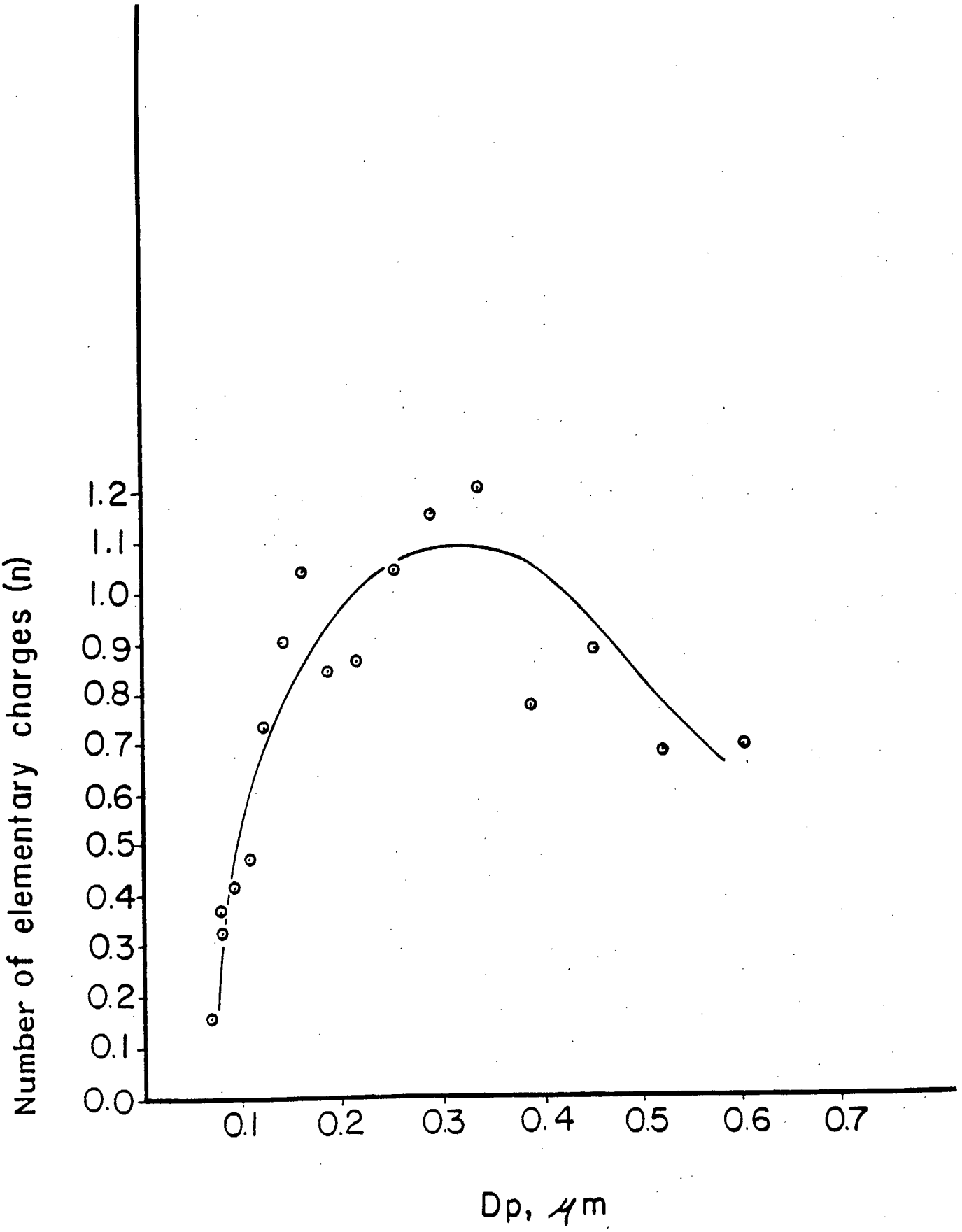

Figure 5. Particle charge versus particle diameter.

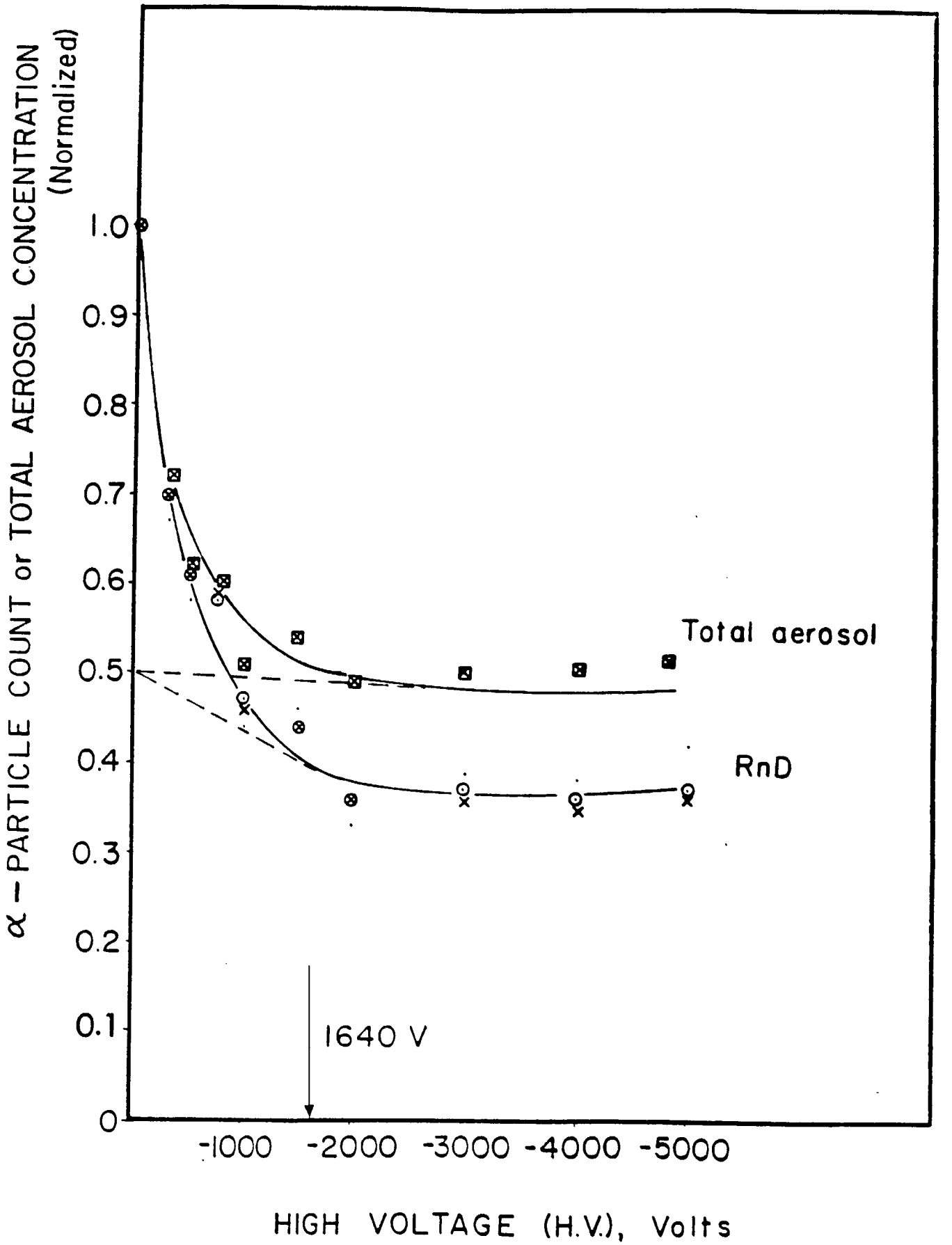

Figure 6. Normalized α-particle count (lower graph: ^{218}Po (.); ^{214}Po (⊙); total α-particle activity (x)), and 'total' aerosol (⊠) concentration (upper graph) versus SFE voltage. The dotted lines are the tangent lines to the curves, drawn from the 0.5 point, to determine V_o (see text).

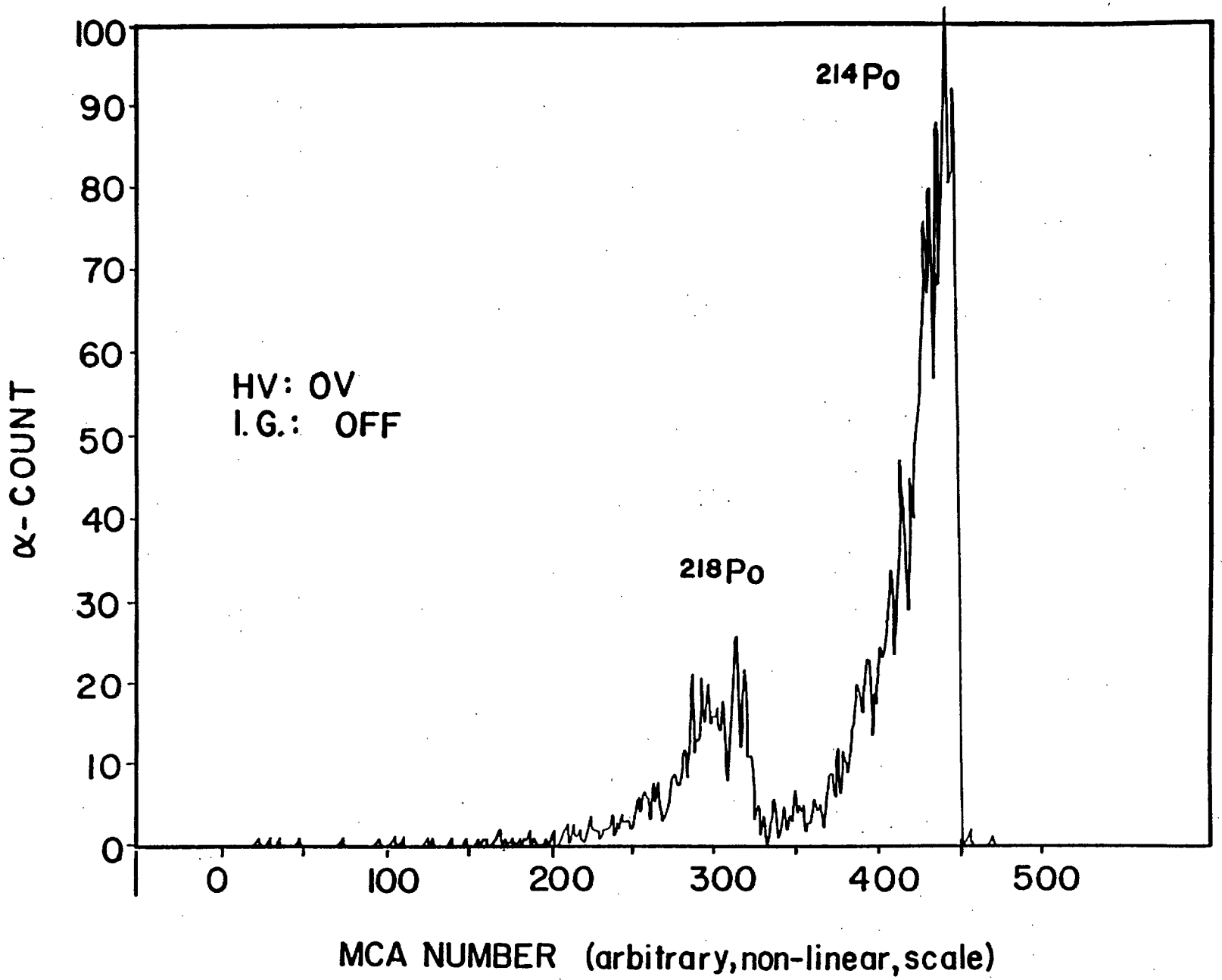

Figure 7a. Alpha-particle spectrum at the outlet of the SFE for H.V. = 0 V and IG off.

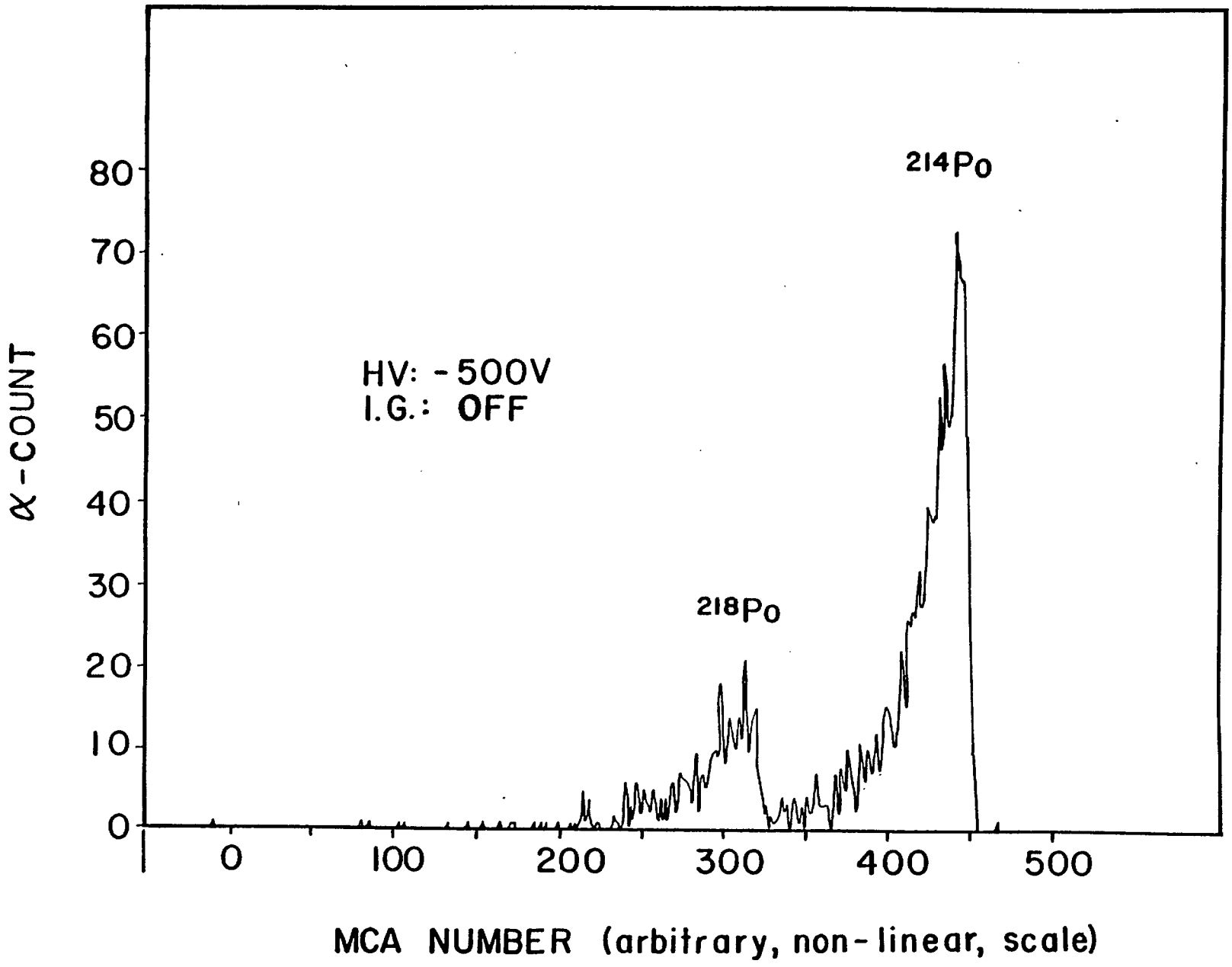

Figure 7b. Alpha-particle spectrum at the outlet of the SFE for H.V. = -500 V, and IG off.

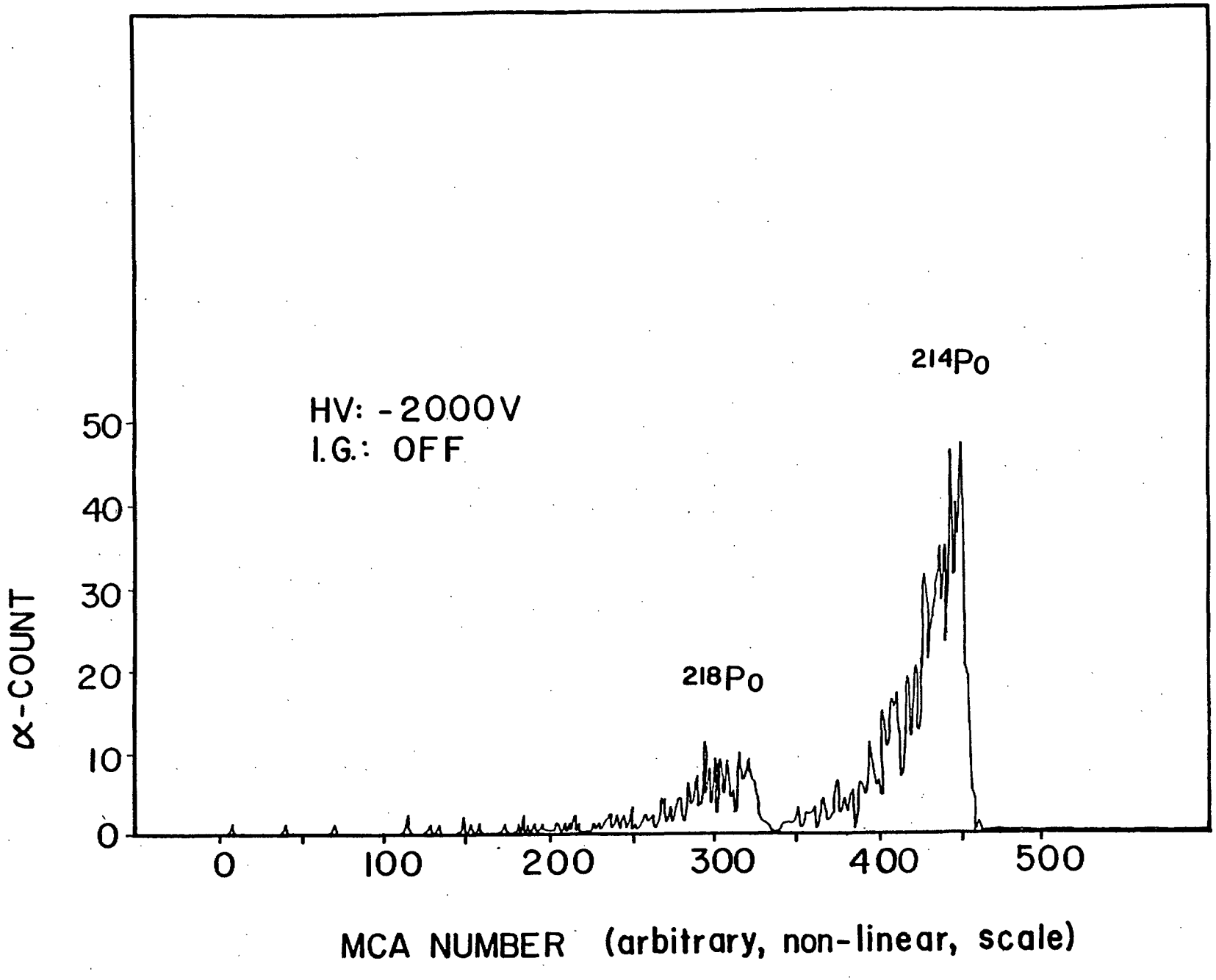

Figure 7c. Alpha-particle spectrum at the outlet of the SFE for H.V. = -2000 V and IG off.

Figure 8. Total aerosol concentration versus SFE voltage for an aerosol cloud exposed to a negative ion-generator. Data obtained using configuration Y (see Fig. 2). The right hand side scale of the y-axis indicates normalized values for the aerosol concentration. The dotted lines are the tangent lines to the positive and negative parts of the curve, drawn from the 0.5 point, to determine the V_o's (see text).

Figure 9. Particle size and mobility distribution for an aerosol cloud exposed to a negative ion generator. (For an explanation of the variables B^+-A and B^--A, see text.)

Figure 10. Total aerosol size and concentration distributions in the RTTF with IG off and on (left hand side histograms, top and bottom, respectively). Also shown are data at the outlet of the SFE for H.V. = -5000 V with IG off and on (right hand side histograms).

Figure 11. Normalized α-particle count versus SFE voltage for ^{218}Po, ^{214}Po, and total α-particle count ($N_{\alpha,T}$).

Figure 12. Normalized total aerosol concentration (N) and α-particle count ($N_{\alpha,T}$) versus SFE voltage. The dotted lines are the tangent lines to the curves, drawn from the 0.5 point, to determine V_o (see text).

Figure 13. Alpha-particle spectra at the outlet of the SFE for H.V. = 0 V, and IG off (top) and IG on (bottom). Aerosol cloud exposed to a negative ion-generator.

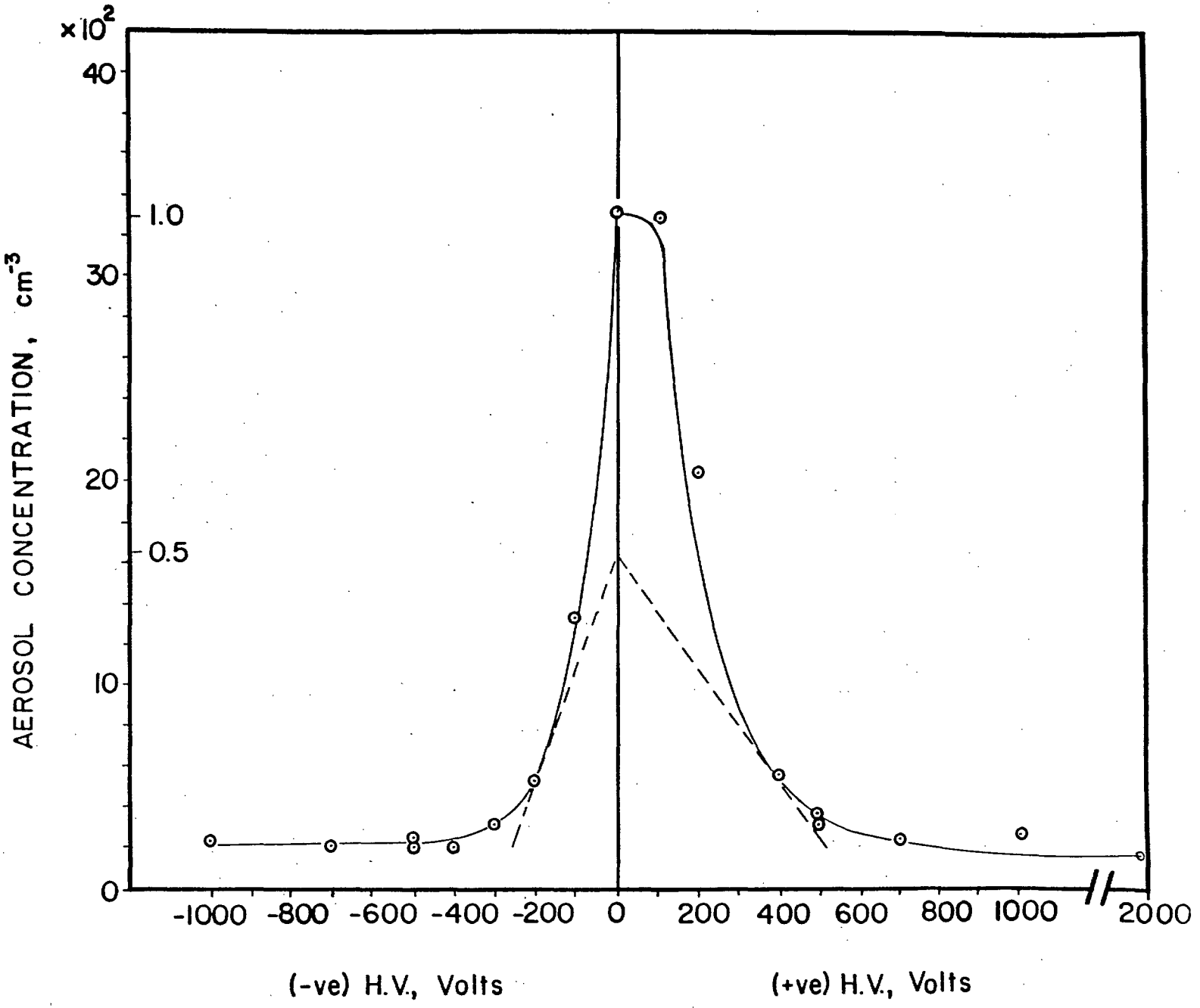
×10²
40
30
20
10
0
1.0
0.5
AEROSOL CONCENTRATION, cm⁻³
-1000 -800 -600 -400 -200 0 200 400 600 800 1000 2000
(-ve) H.V., Volts
(+ve) H.V., Volts

Figure 8

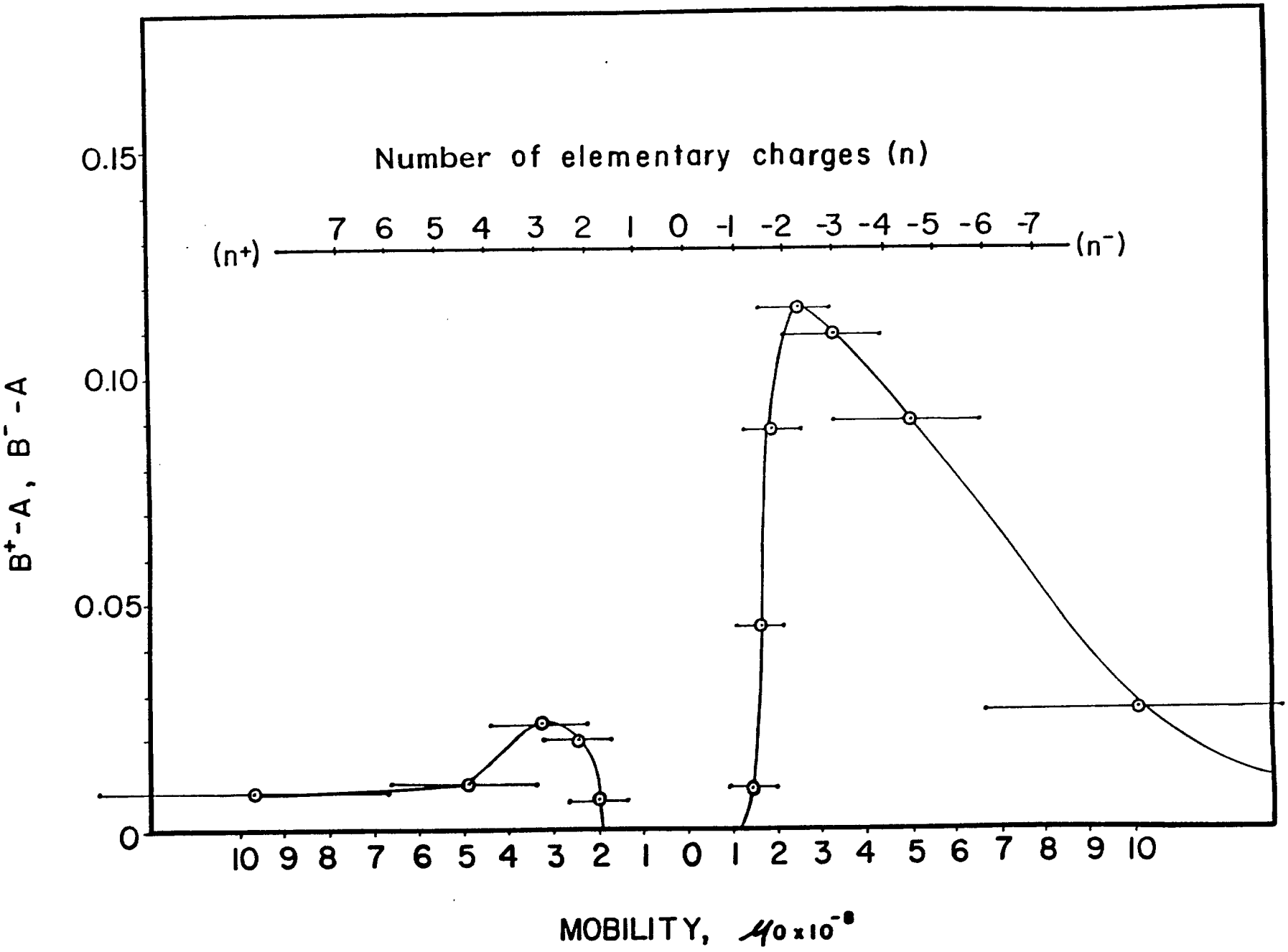
Number of elementary charges (n)
7 6 5 4 3 2 1 0 -1 -2 -3 -4 -5 -6 -7
(n+)
(n⁻)
0.15
0.10
0.05
0
B⁺-A, B⁻-A
10 9 8 7 6 5 4 3 2 1 0 1 2 3 4 5 6 7 8 9 10
MOBILITY, μ0 x 10⁻⁸

Figure 9

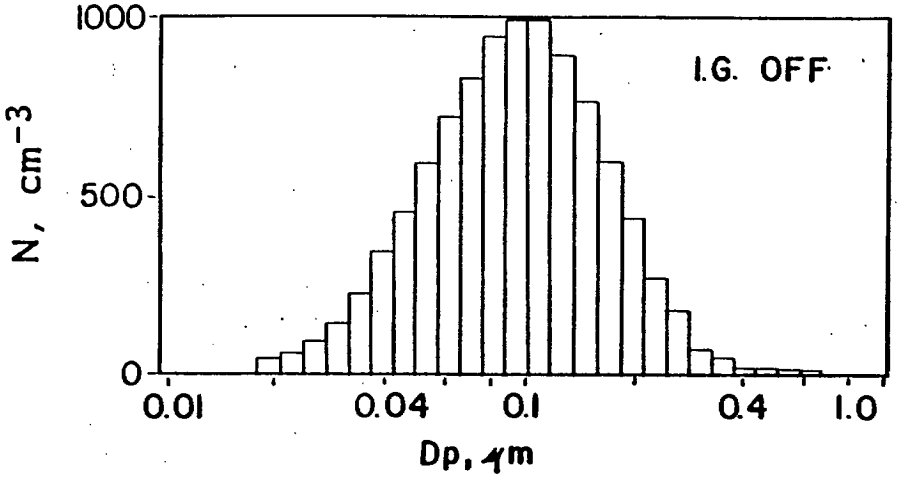
1000
500
0
N, cm⁻³
I.G. OFF
0.01
0.04
0.1
0.4
1.0
Dp, μm

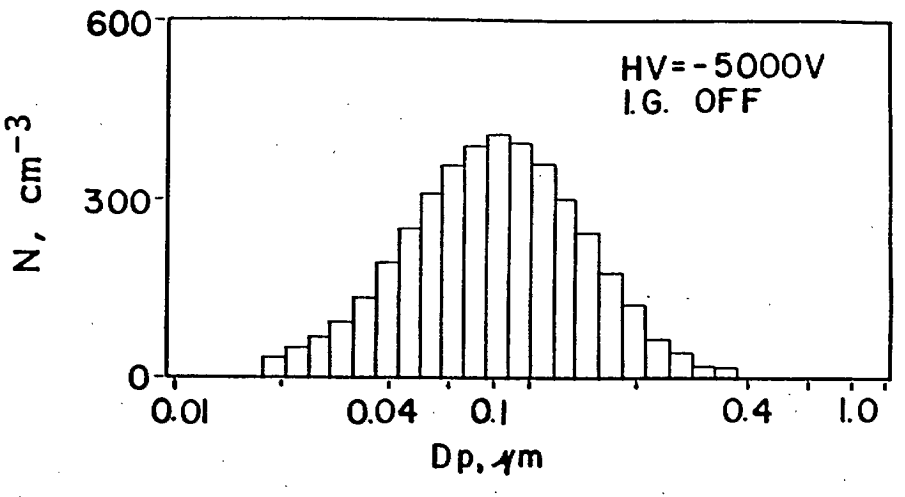
600
300
0
N, cm⁻³
HV=-5000V
I.G. OFF
0.01
0.04
0.1
0.4
1.0
Dp, μm

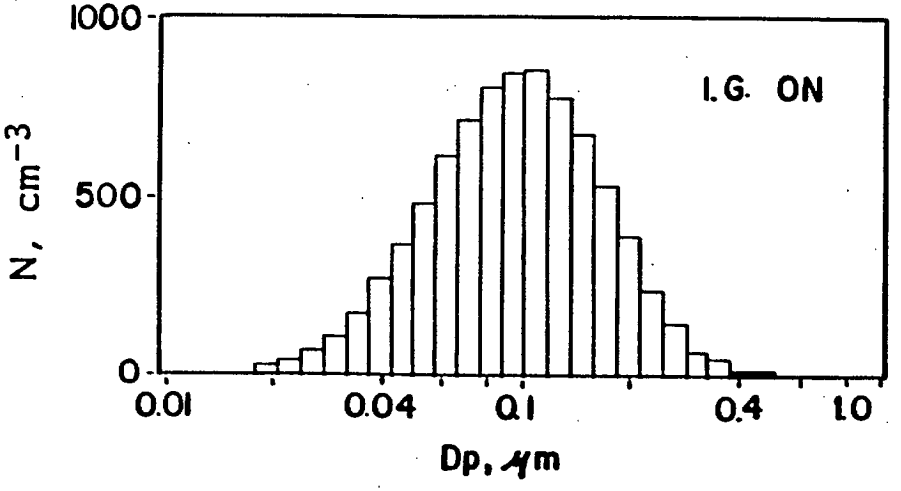
1000
500
0
N, cm⁻³
I.G. ON
0.01
0.04
0.1
0.4
1.0
Dp, μm

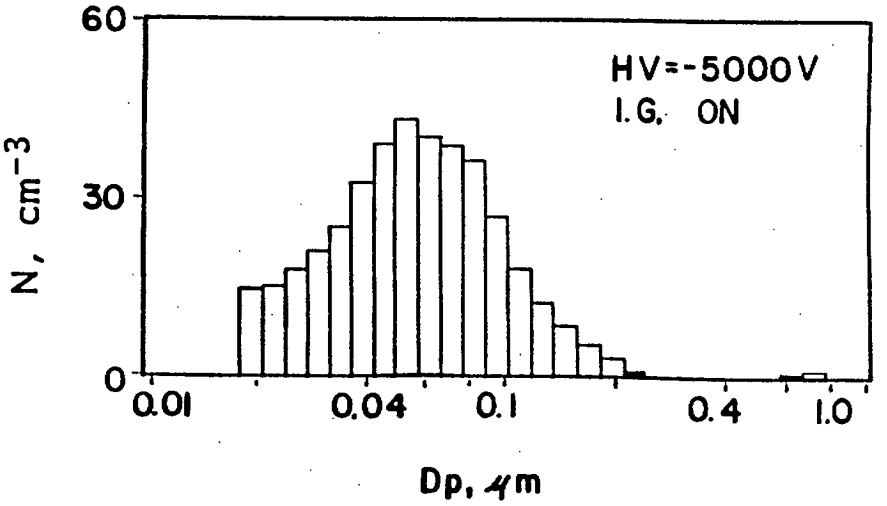
60
30
0
N, cm⁻³
HV=-5000V
I.G. ON
0.01
0.04
0.1
0.4
1.0
Dp, μm

Figure 10

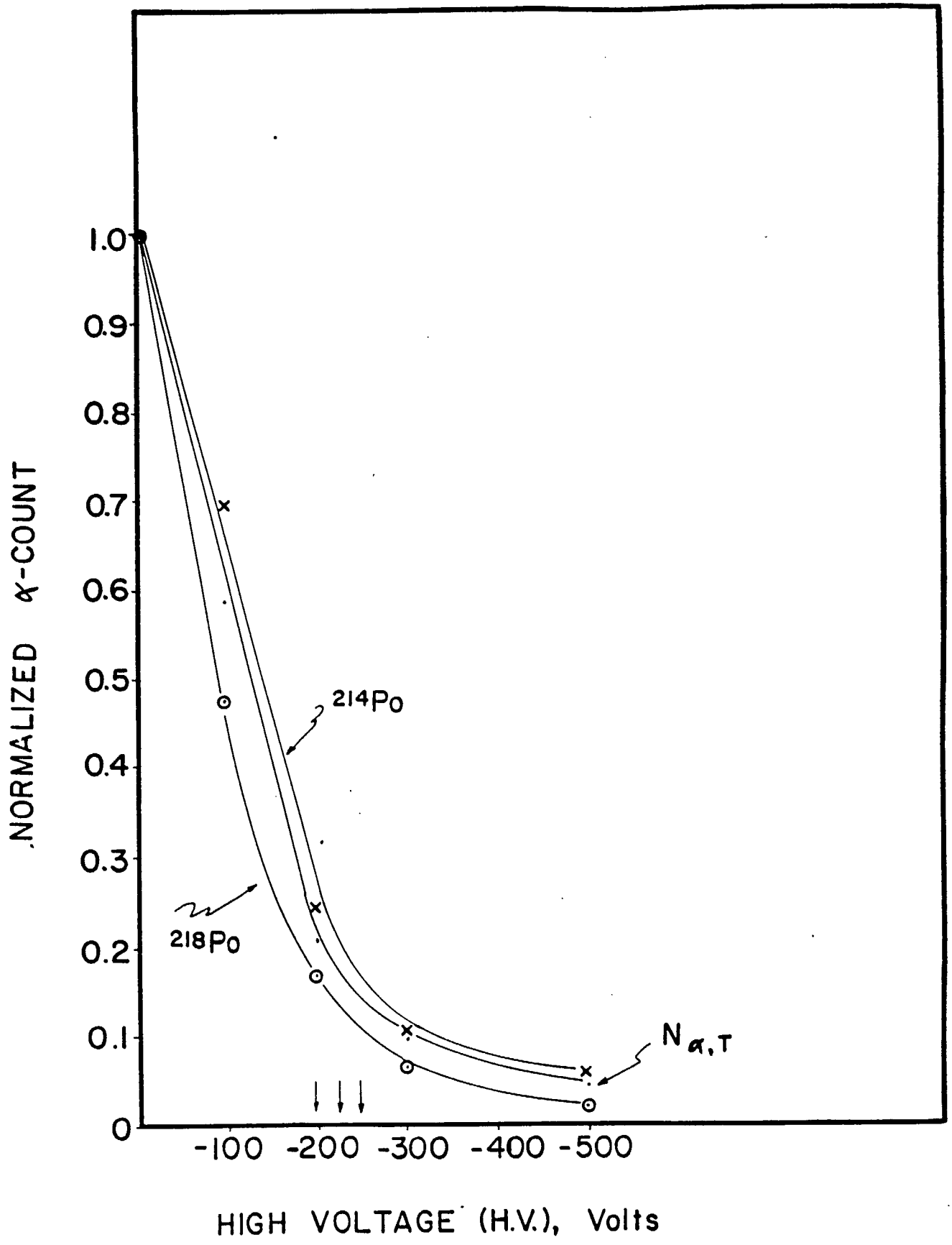
NORMALIZED α-COUNT
1.0
0.9
0.8
0.7
0.6
0.5
0.4
0.3
0.2
0.1
0
214Po
218Po
Nα,T
-100 -200 -300 -400 -500
HIGH VOLTAGE (H.V.), Volts

Figure 11

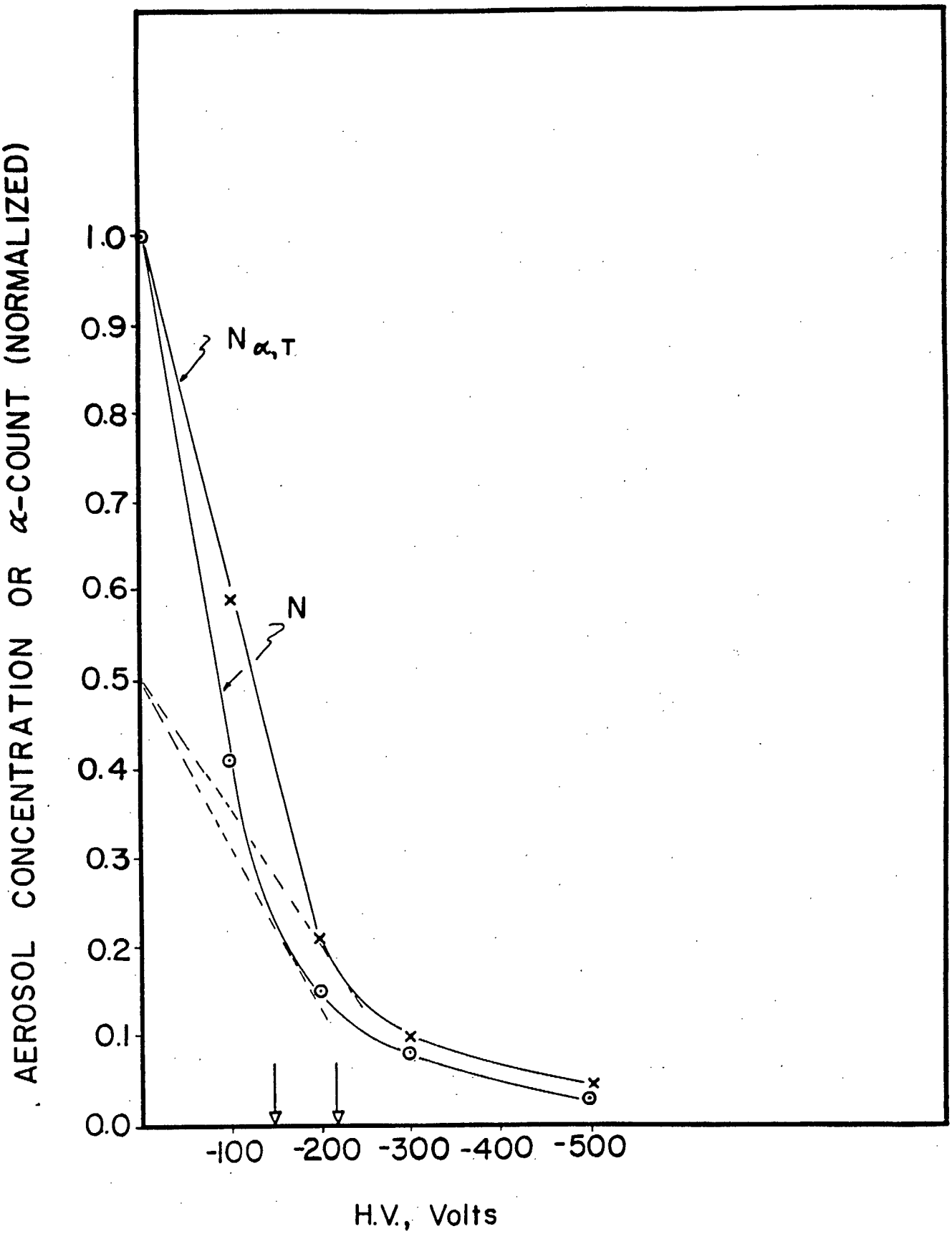
AEROSOL CONCENTRATION OR α-COUNT (NORMALIZED)
1.0
0.9
0.8
0.7
0.6
0.5
0.4
0.3
0.2
0.1
0.0
N α,T
N
-100
-200
-300
-400
-500
H.V., Volts

Figure 12

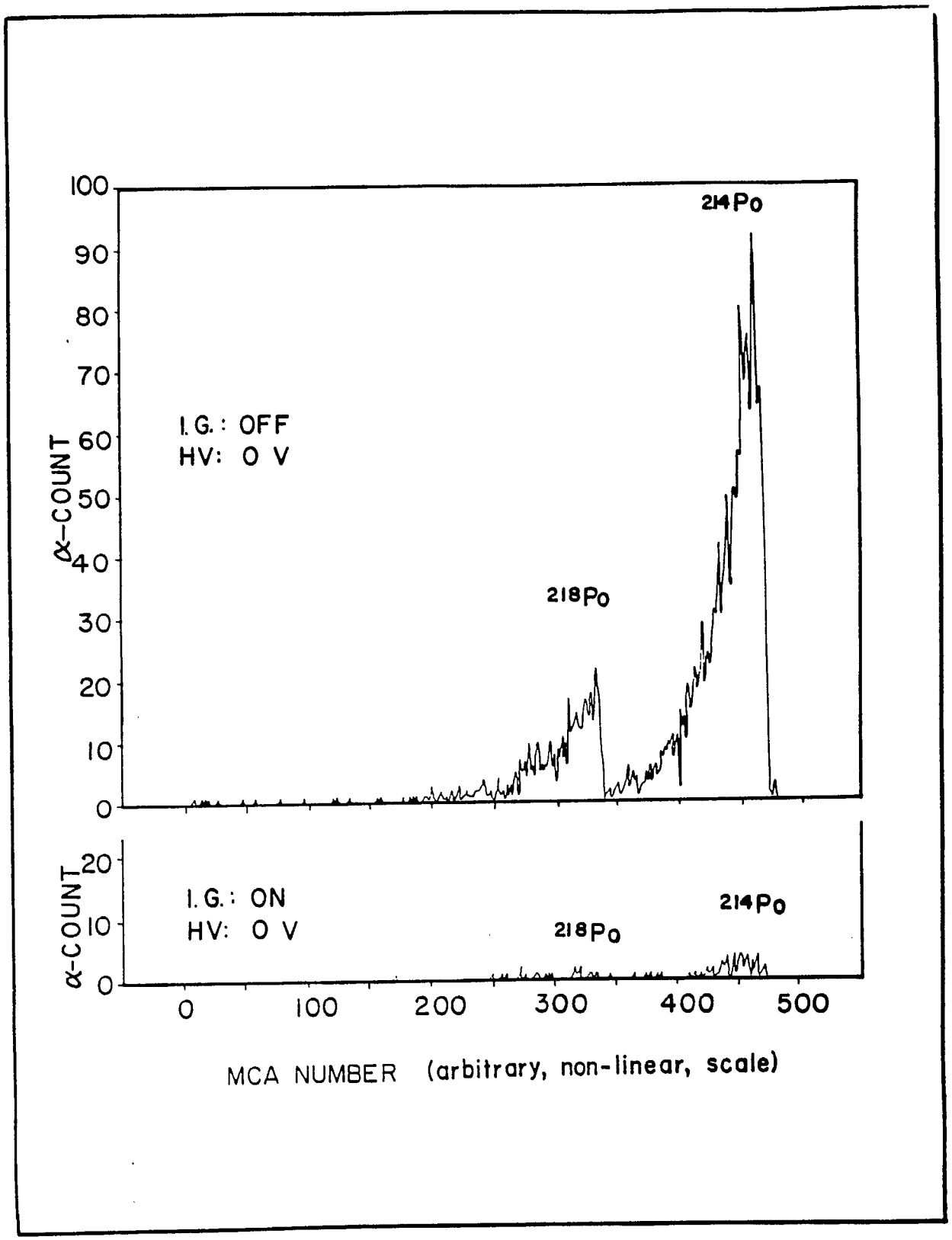
100
90
80
70
60
50
40
30
20
10
0
α-COUNT
I. G. : OFF
HV: 0 V
214Po
218Po
20
10
0
α-COUNT
I. G. : ON
HV: 0 V
214Po
218Po
0
100
200
300
400
500
MCA NUMBER (arbitrary, non-linear, scale)

FIgure 13